ACS Chemical Neuroscience

Research Article

pubs.acs.org/chemneuro

Amyloid Properties of Asparagine and Glutamine in Prion-like Proteins

Yuan Zhang, Viet Hoang Man, Christopher Roland, and Celeste Sagui*

Department of Physics, and Center for High Performance Simulations (CHiPS), North Carolina State University, Raleigh, North Carolina 27695, United States

Supporting Information

ABSTRACT: Sequences rich in glutamine (Q) and asparagine (N) are intrinsically disordered in monomeric form, but can aggregate into highly ordered amyloids, as seen in Q/N-rich prion domains (PrDs). Amyloids are fibrillar protein aggregates rich in β-sheet structures that can self-propagate through protein-conformational chain reactions. Here, we present a comprehensive theoretical study of N/Q-rich peptides, including sequences found in the yeast Sup35 PrD, in parallel and antiparallel β-sheet aggregates, and probe via fully atomistic molecular dynamics simulations all their possible steric-zipper interfaces in order to determine their protofibril structure and their relative stability. Our results show that polyglutamine aggregates are more stable than polyasparagine aggregates. Enthalpic contributions to the free energy favor the formation of polyQ protofibrils, while entropic contributions favor the formation of polyN protofibrils. The considerably larger phase space that disordered polyQ must sample on its way to aggregation probably is at the root of the associated slower kinetics observed experimentally. When other amino acids are present, such as in the Sup35 PrD, their shorter side chains favor steric-zipper formation for N but not Q, as they preclude the in-register association of the long Q side chains.

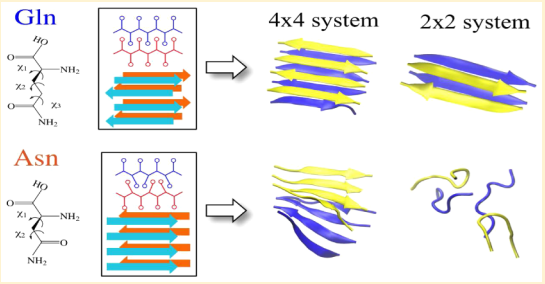

KEYWORDS: *Prion, amyloid, protein aggregation, intrinsically disordered proteins, polyglutamine disease*

1. INTRODUCTION

Eukaryotic proteomes are rich in "low-complexity" sequences, which are distinguished by the prevalence of certain amino acids.[1,2] These sequences lack well-defined three-dimensional structures and thus are under-represented in the RCSB PDB.[3] In general, these sequences are quite abundant (14% of the proteins of *Homo sapiens* include at least one simple sequence[4]) and involve either single amino-acid repeats or a few different amino acids. Variations in the length of the sequences are a source of quantitative genetic variation in evolution but can also cause severe diseases in humans. In particular, sequences rich in glutamine (Q) and asparagine (N) are intrinsically disordered in monomeric form,[5−7] but can aggregate into highly ordered amyloids.[8,9] Amyloids are fibrillar protein aggregates rich in β-sheet structures that can self-propagate through protein-conformational chain reactions. Pure polyglutamine (polyQ) stretches in humans are associated with at least nine late-onset progressive neurodegenerative diseases, which are caused by polyQ expansions greater than a given threshold in proteins with little or no similarity except for the polyQ region. For instance, in Huntington's disease, the normal polyQ length in Huntingtin (Htt) is 10−34 repeats, and pathological lengths are 36−120 repeats. Although each disease has a different pathology, they all share some common feature such as the formation of polyQ aggregates,[10] and eventual neuronal death. Many structural models have been proposed for polyQ aggregates, such as α-helical coiled coils,[11] β-helices,[12] α-sheets,[13,14] and β-sheets.[15,16] Current evidence based on polyQ fibers and crystallites supports the presence of cross-β structures,[15−20] common to other amyloid fibrils. PolyQ expansions occur at the DNA level as a consequence of the unstable expansion of CAG codons.

By contrast, prion diseases can have a genetic, infectious, or sporadic origin that involves modification of the prion protein (PrP). This also results on fatal neurodegenerative diseases such as Creutzfeldt−Jakob (CJD) and Straussler−Scheinkerd diseases of humans, bovine spongiform encephalopathy (BSE), and scrapie of sheep. The cellular prion protein (PrP^C) is encoded by a gene, and a post-translational modification converts it into the infectious abnormal isoform, (PrP^{Sc}), which is rich in β-sheet content.[21] Independently of whether the presence of PrP^{Sc} in the cell is the product of a post-translation mishap or whether it is an external infectious agent, PrP^{Sc} acts as a template upon which PrP^C further aggregates thus enabling the non-Mendelian inheritance characteristic of prions. Prions also cause non-Mendelian inheritance in yeast, which has become a very important model system for the study of prions. Aggregation-prone, Q/N rich domains are present in the baker's yeast *Saccharomyces cerevisiae*, in proteins such as Sup35p and Ure2p, whose amyloid prions are [PSI^+] and [*URE*3], respectively. Although prions can cause disease in yeast, cells with certain

Received: December 18, 2015
Accepted: February 25, 2016
Published: February 25, 2016

DOI: 10.1021/acschemneuro.5b00337
ACS Chem. Neurosci. 2016, 7, 576−587

prion forms have been shown to survive better under adverse conditions, which supports the view that at least some prions developed under positive evolutionary selection.[22] In this sense, fungal prions belong to the category of functional amyloids, such as those found for instance in biofilms in bacteria: HET-s fibrils of Podospora anserina, required by heterokaryon incompatibility;[23] the chaplin peptides from the bacterium *Streptomyces coelicolor*, associated with fimbriae formation;[24] as well as curli fibrils of *Escherichia coli* and *Salmonella enterica* with adhesive function.[25]

One important research direction in the characterization of prions involves the investigation of the relative roles of the polar, uncharged residues Q and N in Q/N-rich yeast prions.[6,26−28] As an example, a recent study found opposing effects of Q and N in the formation of the Sup35 prion-forming domain (PrD).[28] The experiments found that if all the Ns in the wild-type Sup35 PrD were switched to Qs, then amyloid formation decreased but toxicity to the cell increased. Conversely, switching all Qs to Ns enhanced benign, self-templating amyloid formation and decreased cell toxicity.[28] The correlation between the lack of amyloid formation and increased toxicity for polyQ sequences is supported by a large body of literature in neurodegenerative polyQ diseases, where the formation of aggregates and toxicity in neuronal cells are not believed to be linked as cause-effect as was once thought.[29] Instead, it is believed that the formation of large aggregates represents a cellular protective response against further toxicity,[29−31] and that it is the soluble monomeric or oligomeric intermediates that are toxic to the cell.

A complete understanding of the mechanisms of polyQ toxicity still eludes us. However, one can address structural, thermodynamic and kinetic issues related to the amyloids themselves; for instance, why would N-rich sequences form amyloid-like prions while Q-rich sequences would not? The results obtained for the Sup35 PrD[28] were unexpected because it was previously thought Qs and Ns are equivalent in terms of prion formation,[32,33] and because algorithms for recognizing amyloidogenic sequences neither provide a distinction for the effects of Q and N switching nor predict amyloid formation for the Q/N-rich PrD.[28] Since these experiments did not have atomic resolution, Monte Carlo simulations were employed in search for an atomistic explanation of these results. The results of the simulations of Q_{30} and N_{30} homopolymers suggested that the N-rich sequences increase the formation of β-hairpin turns and thus of β-sheets, which in turn would lead to the formation of the N-rich amyloids. A more recent study employs several biophysical tools to characterize and compare the aggregation kinetics of N_{24} and Q_{24} peptides.[34] The main finding is that the kinetics of aggregation of N_{24} is much faster than that associated with Q_{24}.

In this work, we seek to study and compare the fibril structural characteristics of Asn and Gln amino acids. We carry out molecular dynamics (MD) simulations that complement and integrate previous experimental and simulation results on N/Q-rich sequences. Particularly, our work presents the first comprehensive theoretical study of all the possible interfaces, structures and relative stability of the important N/Q-rich peptides (including sequences found in the yeast Sup35 prion domain), as they form amyloid-like protofibrils. We explore all possible steric zipper interfaces for N-rich and Q-rich oligomers in order to determine which crystallographic class[35] provides the most stability to the N-rich or Q-rich fibril precursor. Our observations can be summarized as follows. First, different crystal classes maximize stability in N-rich or Q-rich aggregates. By comparing the most stable (in their optimum class) fibril precursor aggregates, we show that polyQ aggregates are more stable than polyasparagine (polyN) aggregates. Second, the presence of β-hairpin turns in polyN leading to β-sheets not necessarily explains the observed trend of polyN faster aggregation, since N-rich sequences tend to favor parallel β-sheets, as opposed to antiparallel ones, and β-hairpin turns are more stable in polyQ than in polyN. In particular, tight hairpin turns in polyQ have been recently observed experimentally.[18,19] In our previous work, we have measured a non-negligible comparable population of *loose* turns both in disordered polyQ[7] and in disordered polyN,[36] and other simulations have also found polyQ β hairpins.[37] Third, enthalpic contributions to the free energy favor the formation of polyQ protofibrils, while entropic contributions favor the formation of polyN protofibrils. Fourth, when other amino acids are present, such as in the Sup35 PrD, their shorter side chains favor steric-zipper formation for N but not Q, as they preclude the in-register association of the long Q side chains.

2. RESULTS AND DISCUSSION

2.1. Initial Structures. The purpose of our investigations is to contrast the differing roles played by Gln and Asn in the formation of intraneuron protein aggregates. We have therefore investigated the stability of various aggregate models that are compatible with the experimental data, specifically as it pertains to the yeast prion protein Sup35.[35] Specifically, the steric interfaces characterizing the amyloids are based on parallel or antiparallel cross-linked β-sheets with various crystal symmetries and side-chain interdigitation. The structures considered therefore represent a generalization of the experimental structures (as originally proposed, for instance, in ref 15), accounting for all possible symmetries and the possible presence of different amino acids. We also note that we have previously investigated polyQ structures with larger number of residues[20] (i.e., polyQs with arcs and turns) with results that are in good agreement with the experimental studies.[15] To understand our results, it is important that we first discuss the different models considered, and the nomenclature that is used to describe them. The models investigated are listed in Table 1, and a description of their construction is to be found in the Supporting Information (SI). Model 2010 in Table 1 is then used to generate 29 different models (all in "class A", see below) mainly with mutations of one or two Qs into Gs.

The models introduced here are based on a set of $M \times N$ oligomeric crystals, with integer M representing the number of strands in a sheet and integer N the number of sheets in a given oligomer. The simplest structures we considered are the 2×1 homopolymers Ace-Gln_{23}-Nme and Ace-Asn_{23}-Nme, corresponding to an antiparallel β-sheet connected by a "hairpin".

The majority of the structures considered are based on 4×2 and 2×2 model aggregates, which fall into two categories each (4T, 4O and 2T, 2O series) based on their side-chain packing. The aggregate structure itself is based on the classification proposed by Sawaya et al.,[35] who proposed eight classes of rigid steric zippers according to the relative positions of the β strands and sheets. Aggregates are classified according to whether (i) sheets are made from parallel or antiparallel strands; (ii) the adjacent sheets are packed with the same ("face-to-face") or reverse ("face-to-back") surfaces; and (iii) the symmetry operation used to generate the second sheet from the first preserves the order of the strands, such that the upper and lower strands in one sheet are still in that order ("up−up") in the second sheet, or inverts it ("up−down"). A schematic of the eight

DOI: 10.1021/acschemneuro.5b00337
ACS Chem. Neurosci. 2016, 7, 576−587

Table 1. Characterization of the Initial Conformations

system size	model name	sequence	sheet	class	side chain
2 × 1 (hairpin)	Q_{23}	Ace-Gln_{23}-Nme	antiparallel		
	N_{23}	Ace-Asn_{23}-Nme	antiparallel		
4 × 2	4T1	GNNQQNY	parallel	1	2-by-2
	4T2	GNNNNNY	parallel	1	2-by-2
	4T3	NNNNNNN	parallel	1	2-by-2
	4T4	GQQQQQY	parallel	1	2-by-2
	4T5	SNQNNF	parallel	2	2-by-2
4 × 2	4O1	NNNNNNN	parallel	1	1-by-1
	4O2	QQQQQQQ	parallel	1	1-by-1
	4O3	NNNNNNN	parallel	4	1-by-1
	4O4	QQQQQQQ	parallel	4	1-by-1
	4O5	NNNNNNN	parallel	3	1-by-1
	4O6	QQQQQQQ	parallel	3	1-by-1
	4O7	NNNNNNN	parallel	2	1-by-1
	4O8	QQQQQQQ	parallel	2	1-by-1
	4O9	NNNNNNN	antiparallel	A	1-by-1
	4O10	QQQQQQQ	antiparallel	A	1-by-1
2 × 2	2T1	GNNQQNY	parallel	1	2-by-2
	2T2	GNNNNNY	parallel	1	2-by-2
	2T3	NNNNNNN	parallel	1	2-by-2
	2O2	QQQQQQQ	parallel	1	1-by-1
	2O4	QQQQQQQ	parallel	4	1-by-1
	2O9	NNNNNNN	antiparallel	A	1-by-1
	2O10	QQQQQQQ	antiparallel	A	1-by-1

possible classes of aggregate models is shown in Figure 1. In addition to these considerations, one can consider two more criteria based on the type of side-chain packing, as shown in Figure 2c. In the "1-by-1" packing the side chains of two adjacent sheets intercalate with each other "one-by-one" as in a true zipper, while in the "2-by-2" packing two side chains intercalate every second set of side chains. The "One-by-One" packing gives rise to the 4O and 2O sets of models, while the "two-by-two" packing is associated with the 4T and 2T sets.

The number of steric zipper classes reduces considerably when (not too short) homopeptides are considered, as shown in Figure 2. In this case, the "face-to-face" and "face-to-back" structures are the same for the parallel sheets, and the first four classes of Sawaya et al.[35] are reduced to two: aggregates with parallel-stranded sheets in which the sheets are either parallel (class 2 and class 3) or antiparallel (class 1 and class 4) with respect to each other. In class 1 = 4, the carboxamide dipoles in polyN or polyQ are aligned at the interface between the two sheets, while in class 2 = 3, the dipoles in one sheet point in the opposite direction to those in the other sheet. Concerning steric zippers in antiparallel sheets (classes 5 to 8), for (not too short) homopeptides classes 6 to 8 reduce to a single structure, where the strands facing each other in opposite sheets point in the same direction (i.e., the two sheets are stacked in a parallel way), while class 5 (which so far has not been observed experimentally) corresponds to two sheets stacked in an antiparallel way. Furthermore, antiparallel-stranded sheets in polyQ tend to shift with respect to each other such that the strands of different sheets no longer lie on top of each other, but "in-between" each other in a zipperlike fashion. This is known as "quarter-stagger" in β-sheet crystals, and it has been observed both experimentally and in simulations.[16,20] When this happens, all of Sawaya et al.[35] steric zippers involving antiparallel-stranded sheets (classes 5 to 8) reduce to a single

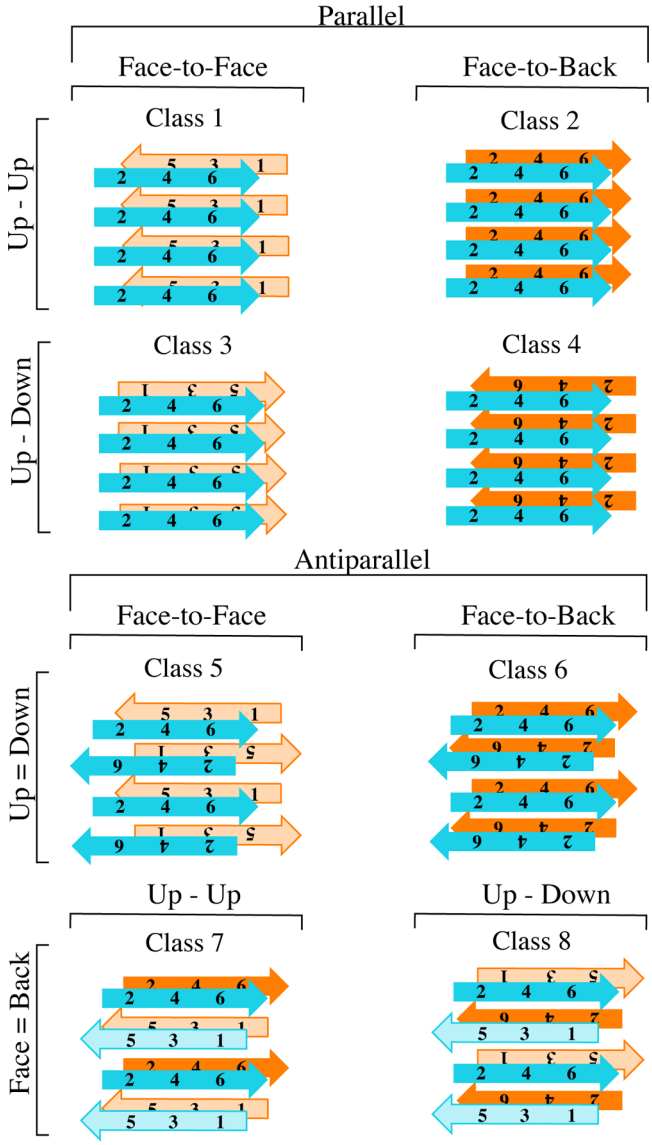

Figure 1. Eight classes of steric zippers, following Sawaya et al.[35] The sheet closer to the viewer is shown in blue, and the one behind in orange. The solid colors show the "front side" of each sheet with the side chains identified by even numbers, and the faded colors show the "back side" of the sheets with odd-number side chains.

structure, which for convenience we here label as class A (for antiparallel sheets).

We now turn to the specific models we investigated, which are listed in Table 1. First, we constructed four models (labeled 4T1 to 4T4) based on the X-ray crystal structure of the GNNQQNY peptide (PDB ID 1YJP).[38] The model 4T1 corresponds exactly to the 1YJP crystal structure with eight GNNQQNY peptides forming two parallel sheets with strands separated by 4.87 Å in each sheet. The sheets therefore reproduce the class 1 steric zipper with "2-by-2" side chain packing in a dry interface with an 8.5 Å separation between the sheets. To study the effects of Q versus N in the formation of Sup35 PrD, we then mutated all the Qs to Ns to obtain 4T2 which was constructed from GNNNNNY strands. Likewise, we also mutated the Ns to Qs to obtain the 4T4 structure, which is based on GQQQQQY strands. Finally, in order to eliminate the effects of the terminal residues G and Y, we mutated these to N to obtain model 4T3 based on NNNNNNN strands. We also constructed one more

DOI: 10.1021/acschemneuro.5b00337
ACS Chem. Neurosci. 2016, 7, 576−587

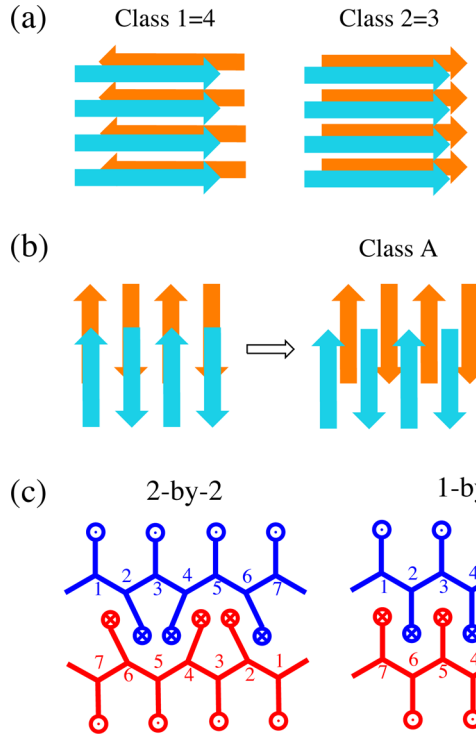

Figure 2. For not too short homopeptides, some of the classes described in Figure 1 converge. (a) For parallel sheets, class 1 and 4 become the same (with sheets stacked in antiparallel fashion), and class 2 and 3 become the same (with sheets stacked in parallel fashion). (b) Schematic of the quarter-stagger displacement of one sheet with respect to the other. For antiparallel sheets undergoing a quarter-stagger, class 5−8 converge into class A (right). (c) Side-chain interdigitation of steric zippers.

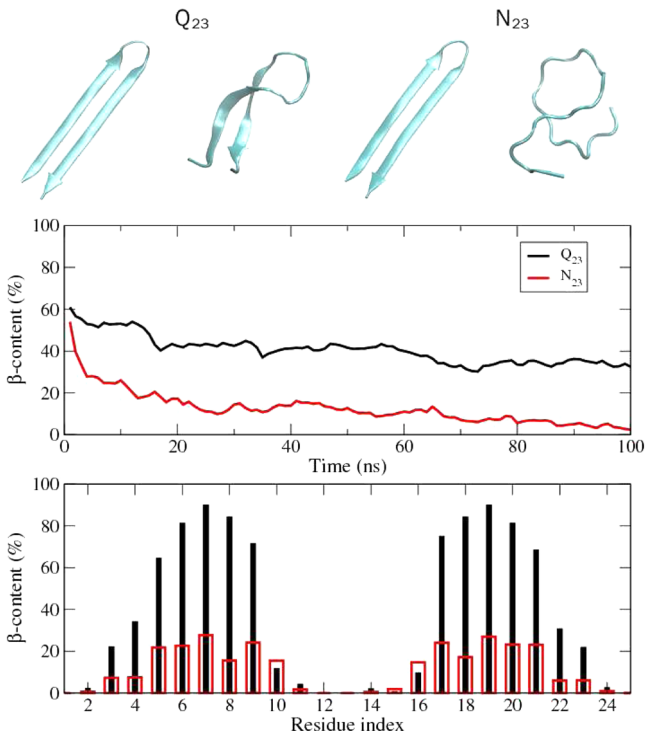

Figure 3. This figure contrasts the relative stability of polyQ versus polyN hairpins. The top panel shows sample initial and final configurations after a 100 ns solvated simulation of Q_{23} and N_{23} β-sheets with an initial β-hairpin (top panel). After 100 ns the polyQ hairpin partially retains its structure, while polyN is disordered. A more quantitative expression is given by the middle panel which gives the percentage of β-sheet content of the hairpins as a function of time, while the bottom panel shows the β-sheet content of each residue averaged over the last 50 ns of the simulation. Here, black and red lines denote results for Q_{23} and N_{23}, respectively, and averages are performed over 10 runs.

structure 4T5, corresponding to the 2OL9 crystal structure with eight SNQNNF peptides forming two parallel sheets with strands separated by 4.79 Å in each sheet. The structure corresponds to class 2 of Sawaya et al.[35]

We also considered aggregates based on the "1-by-1" side-chain packing (the 4O series), obtained from pure polyQ and polyN strands consisting of seven residues so as to be commensurate with the 4T series. Although for longer peptides class 1 coincides with 3, and class 2 coincides with 4, we specifically packed the seven-residue peptides in the four separate symmetries in order to account for possible end effects due to the relative short length of the peptides. Finally, we constructed models 4O9 and 4O10, based on polyN and polyQ strands respectively, arranged in an antiparallel fashion with "1-by-1" side-chain packing.

In order to gain further insight into the stability of these structures, we constructed a number of 2 × 2 models as listed in Table 1. Essentially, these structures were taken from the core strands (which are more stable) in the final configuration of the corresponding 4T or 4O models after a 400 ns simulation in explicit waters. In addition, there are 29 sequences in class A (not listed in Table 1) obtained from mutations in the sequence of 2010.

2.2. Monomeric PolyQ β-Hairpins Are More Stable than Monomeric PolyN β-Hairpins. Figure 3 shows sample initial and final structures (at 100 ns) for the homopolymers Q_{23} and N_{23}. In this and other figures, secondary structure is assigned by DSSP[36] Notice that different secondary structure assignment codes can give different results for conformationally irregular peptides.[36] After 100 ns, Q_{23} still exhibits considerable β sheet structure while N_{23} has become a completely disordered coil. Also shown in Figure 3 is the residue-averaged β content as a function of time (middle), and the time-averaged β content as a function of the residue number (bottom). The data thus suggests that the Q_{23} hairpin is more stable than the N_{23} hairpin. This is an important result, and is in contradiction to the results given in ref 28, which deemed a N_{30} β-hairpin to be more well-defined (leading to a much better antiparallel β-sheet) than the corresponding Q-based structure. The previous simulation results[28] were attributed to the intrinsic difficulty of polyQ sequences to form tight hairpin turns.

Previous Experimental and Simulation Data. Our results are in agreement with previous data. In particular, tight hairpin turns in polyQ have been recently observed experimentally.[18,19] Also, tight β hairpins were proposed and used[16] to successfully model the X-ray diffraction patterns obtained from crystalline fibers and films of a $D_2Q_{15}K_2$ polypeptide.[12] In our own work, we have measured a non-negligible comparable population of loose turns both in polyQ[7] and in polyN,[36] and other simulations have also found polyQ β hairpins.[37] Recent simulations of a Q_{40} monomer (which is above the aggregation threshold for polyQ) containing two tight hairpin turns and an arc turn (a "lateral β-sheetstack") turned out to be remarkably stable in time scales longer than 1 μs.[20]

DOI: 10.1021/acschemneuro.5b00337
ACS Chem. Neurosci. 2016, 7, 576−587

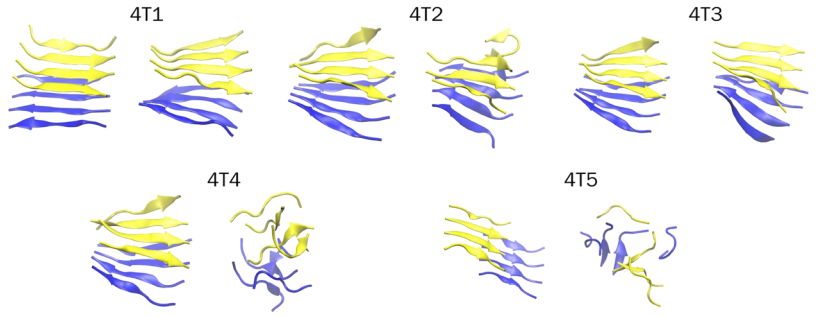

Figure 4. For each 4 × 2 model labeled in the figure and described in Table 1, sample initial configurations after equilibration are shown on the left and sample final configurations at 400 ns are shown on the right.

To conclude, tight β-hairpins and the ensuing antiparallel β-sheets are more stable for polyQ than for polyN.

2.3. N-Rich Oligomers Are Most Stable in "Class 1" Steric Zippers with 2-by-2 Interdigitation. Here we discuss the stability of Q-rich and N-rich models with 2-by-2 side chain interdigitation as schematically shown in Figures 1 and 2. Model 4T1 is based on the experimental PDB 1YJP crystal structure with sequence GNNQQNY, and 4T5 on the experimental 2OL9 crystal structure with sequence SNQNNF. Models 4T1 through 4T4 correspond to class 1 structures: parallel-stranded sheets with face-to-face and up−up packing between the sheets (Figure 1), while model 4T5 corresponds to class 2: parallel-stranded sheet, with face-to-back and up−up packing between the sheets. We also note that although the different 4 × 2 models are constructed from *dry* crystal interfaces as described, the actual simulations of the structures take place in a fully solvated environment.

Sample configurations for the 4 × 2 aggregates are shown in Figures 4 and 5, and sample configurations for the 2 × 2 aggregates are shown in Figure 6. Figures 4 and 5 show initial (after equilibration) and final configurations at 400 ns for each of the 4 × 2 models. Figure 4 shows that N-rich sequences in class 1 structures with 2-by-2 side-chain packing are more stable than the corresponding Q-rich structure. Thus, models 4T1, 4T2, and 4T3 all preserve considerable β-sheet structure after 400 ns, while model 4T4 is completely disordered. Quantitative plots of the time evolution of the structural characteristics of the different models, mainly RMSDs and β-sheet content, are presented in Figures 7 and 8, while intersheet and interstrand distances are given in the SI. Model 4T5 was found to be completely unstable in solution where it lacks the close crystal contacts that stabilize it in crystal environment. Because of the rapid unfolding of this structure in solution, we believe that similar class 2 structures based on pure polyQ and polyN will also be unstable. We would like to notice that, although 4T5 consists of six (as opposed to seven) residues, a 4T3 model with 6 residues per strand (not shown) is still relatively stable. The instability of this model may be the reason why the PDB structure 2OL9 (which forms the basis for model 4T5), appears to be the only class 2 structure with this kind of interdigitation in the PDB databank. More polyN and polyQ class 2 models were investigated in the 4O series, as described below.

Next, we compare the pure polyN structures given by the parallel sheets in the 4T3 and the antiparallel sheets in 4O9 (with a sample configuration shown in Figure 5). Statistically, the RMSDs shown in Figure 7 and the β-sheet contents shown in Figure 8 indicate that the parallel-stranded 4T3 model is more stable than the antiparallel-stranded 4O9 model. This observation is also supported by the intersheet and intrastrand distances

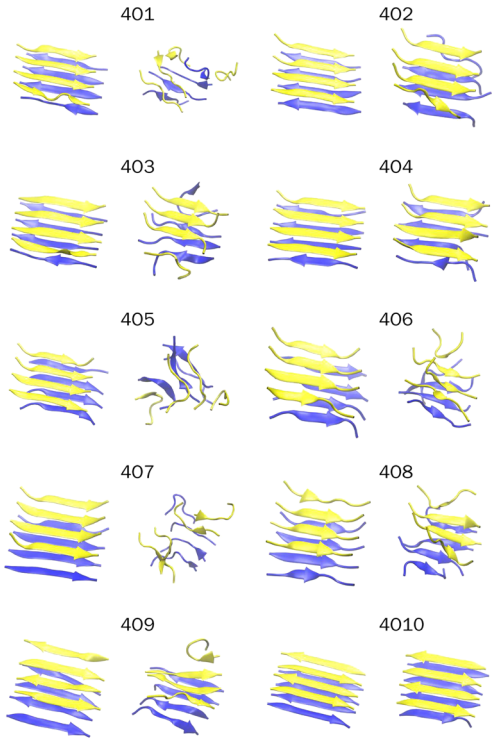

Figure 5. For each 4 × 2 model labeled in the figure and described in Table 1, sample initial configurations after equilibration are shown on the left and sample final configurations at 400 ns are shown on the right. Configurations on the left column correspond to polyN aggregates, and on the right column, to polyQ aggregates.

shown in the SI, Figures S3 and S4. In both cases, the corresponding, smaller 2 × 2 aggregates are unstable.

Previous Experimental and Simulation Data. Our results are in agreement with previous data. The stability of the heptapeptide GNNQQNY in model 4T1 (PDB ID 1YJP[38]) has been confirmed by previous simulations.[39,40] In all cases, the in-register parallel packing of GNNQQNY is consistent with the observed X-ray diffraction data. It has also been pointed out that GNNQQNY exhibits the same amyloid properties as the full-length Sup35, as seen in the cooperative kinetics of aggregation, the binding to the dye Congo red, fibril development, and in the typical cross-β diffraction pattern[38,41] of the structure. The surfaces of the two sheets are complementary resulting in a dry steric zipper with tightly interdigitated side chains. The zipper is stabilized by van der Waals interactions, and hydrogen bonds between the polar groups. Although the π stacking of the aromatic Tyr-Tyr interactions[39] in GNNQQNY plays a role in

DOI: 10.1021/acschemneuro.5b00337
ACS Chem. Neurosci. 2016, 7, 576−587

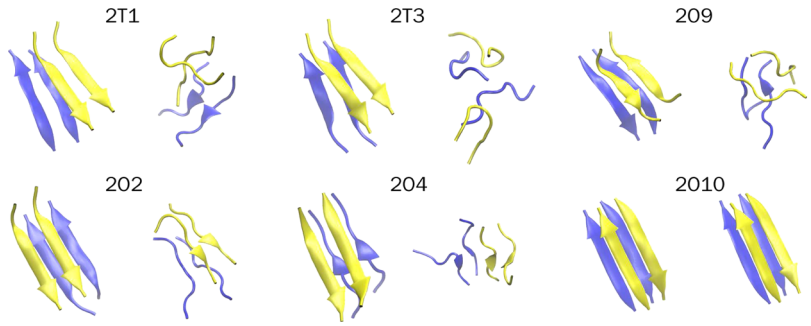

Figure 6. For each 2 × 2 model labeled in the figure and described in Table 1, sample initial configurations after equilibration are shown on the left and sample final configurations at 100 ns are shown on the right. Top row corresponds to polyN aggregates, and bottom row corresponds to polyQ aggregates.

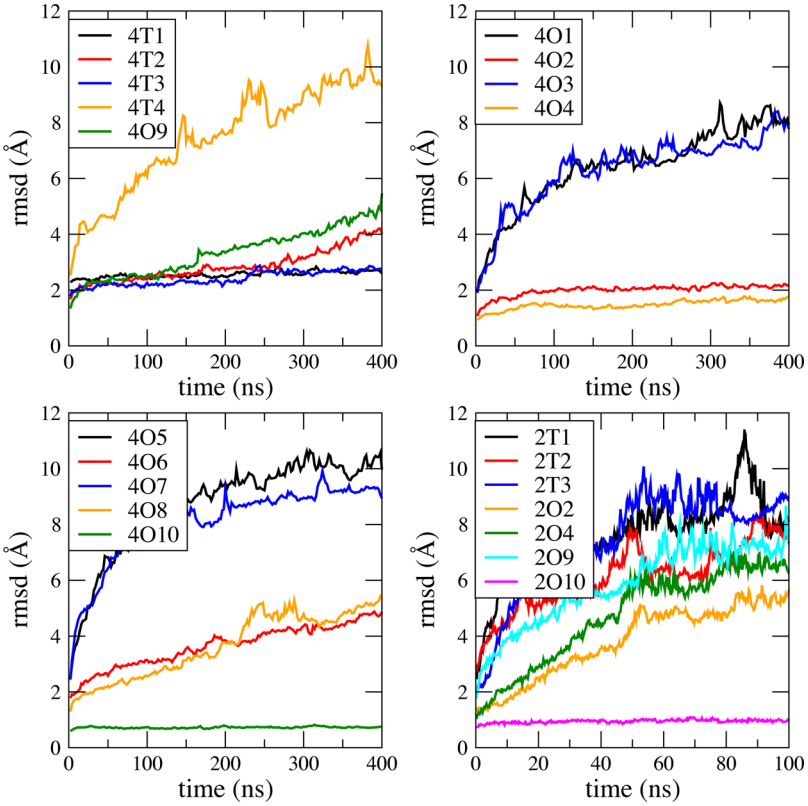

Figure 7. RMSD values of the main chain atoms N, O, C_α and C′ in various models with respect to the corresponding initial structure (after minimization). The values are averaged every 2 ns for 4 × 2 models, and every 0.2 ns for 2 × 2 models, and then averaged over 10 runs.

stabilizing the parallel arrangement of the strands, the pure polyN model 4T3 also favors the formation of this kind of zipper structure. Previously, two single strands of polyN or polyQ homopeptides were shown to assemble in dimers that favor parallel (polyN) or antiparallel (polyQ) β-sheets.[37] In addition, solid-state NMR experiments show that the amyloid of the full prion domain of Sup35p (residues 1−123) has an in-register parallel β-sheet structure.[42]

In summary, N-rich sequences in 4 × 2 aggregates featuring class 1 interfaces with 2-by-2 side-chain packing display stability in the times of the simulations (400 ns). The solution simulation for the sequence in class 2 is not stable for the 4 × 2 model, and therefore, no further mutations are tested. For class 1, the Q-rich model is not stable.

2.4. PolyQ Oligomers Are Most Stable in Antiparallel-Stranded β-Sheets with 1-by-1 Steric Zippers. Next, we turn to structures based on pure polyQ and polyN peptides exhibiting 1-by-1 side-chain packing. As before, we begin our discussion with the 4 × 2 models, as shown in Figure 5. For these models, there are three classes of steric zippers that need to be considered: class 1 = 4 and class 2 = 3 based on a parallel arrangement of strands within a sheet, and class A based on an antiparallel arrangement. However, we specifically packed the peptides in the four separate symmetries in parallel-stranded sheets in order to account for possible end effects due to the relative short length of the peptides.

The results are as follows. First, all the parallel 1-by-1 side-chain classes are unstable for polyN. For polyQ structures, models in class 1 and 4 (4O2 and 4O4) are more stable than the corresponding models in class 2 and 3 (4O6 and 4O8) indicating that an antiparallel packing of parallel-stranded β-sheets is preferred. The final configurations of 4O2 (class 1) and 4O4 (class 4) and their RMSDs in Figure 7 and β-content in Figure 8 are very similar (and so are their intersheet and interstrand

DOI: 10.1021/acschemneuro.5b00337
ACS Chem. Neurosci. 2016, 7, 576−587

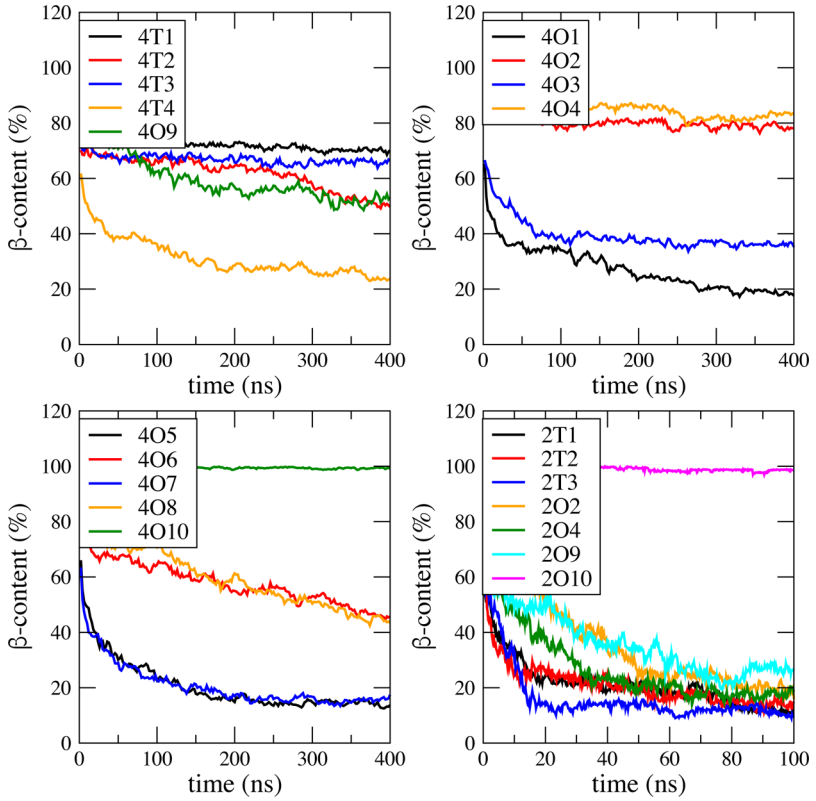

Figure 8. β-Sheet content of the 4 × 2 models 4T1 (black), 4T2 (red), 4T3 (blue), 4T4 (orange), and 4O9 (green) in top left chart; 4 × 2 models 4O1 (black), 4O2 (red), 4O3 (blue), and 4O4 (orange) in top right chart; 4 × 2 models 4O5 (black), 4O6 (red), 4O7 (blue), 4O8 (orange), and 4O10 (green) in bottom left chart; 2 × 2 models 2T1 (black), 2T2 (red), 2T3 (blue), 2O2 (orange), 2O4 (green), 2O9 (cyan), and 2010 (magenta) in bottom right chart. Results are averaged over 10 independent runs.

distances, shown in the SI), suggesting that the end effects are not important and indeed class 1 and class 4 are the same. A similar conclusion is obtained for 4O6 and 4O8, indicating that the end effects in these peptides play no role and class 1 is the same as class 3. Finally, polyQ structures with 1-by-1 side-chain packing and class A zippers (model 4O10) appear to be very stable. PolyN structures with 1-by-1 side-chain packing and class A zippers (model 4O9) also show larger stability than the 1-by-1 side-chain packing polyN parallel arrangements (4O1, 403, 4O5, 4O7). However, the class A polyN model 4O9 is less stable than the 2-by-2 side-chain packing parallel arrangement in 4T3.

Previous Experimental and Simulation Data. Our polyQ results are in complete agreement with current evidence based on polyQ fibers and crystallites supporting the presence of cross-β structures with antiparallel β-sheets.[15−20]

2.5. The Most Stable PolyQ Structures Show Higher Stability than the Most Stable PolyN Structures. At this point, the results for the 4 × 2 aggregates (at 400 ns) include the following relatively stable structures: polyN 2-by-2 class 1 structures (4T1, 4T2, and 4T3) and polyN 1-by-1 class A structure (4O9); and three stable 1-by-1 polyQ structures: class 1 (4O2), class 4 (4O4), and class A (4O10). Figures 7 and 8 suggest that the polyQ structures are more stable. Recognizing that cooperative effects in larger aggregates make them more stable than smaller aggregates,[20] one can build smaller aggregates with the same symmetry and test them for stability. Indeed, in a situation where peptides are undergoing a transition from a disordered state to an amyloid precursor, the higher stability of a small nucleus would confer a higher chance to the formation of the protofibril. Thus, we used the most stable 4 × 2 structures to build the corresponding 2 × 2 models. These are listed in Table 1 and shown in Figure 6 for a sample configuration, while the time evolution is shown in Figures 7 and 8.

The reduction in size causes the 2 × 2 aggregates for class 1 models with 2-by-2 side-chain packing (i.e., GNNQQNY in 2T1, GNNNNNY in 2T2, and NNNNNNN in 2T3) to quickly become unstable. So does the polyN structure in the antiparallel, class A, 1-by-1 model 4O9. A previous simulation of GNNQQNY oligomers also found that these were unstable when in 2 × 2 aggregates.[43] For polyQ, the 1-by-1 class 1 (2O2) and class 4 (2O4) also become unstable. On the other hand, the 1-by-1 class A (2010) model is very stable.

All the models probed here have "reactive", rigid, edge strands with exposed main-chain hydrogen bond donors and acceptors which would drive the elongation of fibrils after a size threshold.[44,45] This same reactivity makes all the small 2 × 2 oligomers unstable, except for 2010. This feature is peculiar to polyQ, which in the 1-by-1 class A model exhibits tightly interdigitated side chains, stabilized not only by dipole−dipole interactions, and backbone−backbone, interside−chain, and backbone−side-chain hydroden bonds, but also by strong van der Waals interactions between the closely fitting side chains.[16,20]

Previous Experimental and Simulation Data. We are not aware of studies comparing the stability of polyN and polyQ amyloid-like aggregates.

Melting by a Free-Electron Laser Pulse. Recently, free electron lasers have been used for melting biomolecular complexes.[46,47] Kawasaki and co-workers[47] have developed a mid-infrared free electron laser with highly specific oscillation characteristics having a high photon density, a picosecond pulse

DOI: 10.1021/acschemneuro.5b00337
ACS Chem. Neurosci. 2016, 7, 576−587

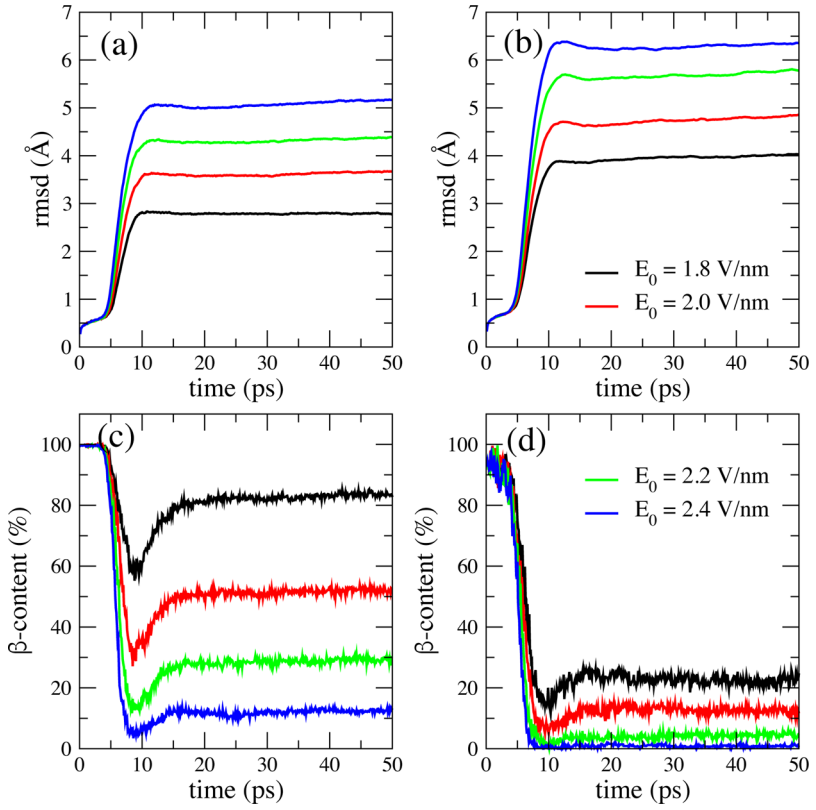

Figure 9. Time dependence of the RMSD and β-sheet content (taken with respect to the initial structure) of model 4O10 (panels a,c) and 4T3 (panels b,d) subject to an infrared laser pulse with modulus of the electric field amplitude corresponding to E_0 = 1.8 (black), 2.0 (red), 2.2 (green), and 2.4 (blue) V/nm, respectively.

structure, and a range of tunable frequencies. To date, such a laser pulse with frequencies tuned to the amide I bands has been used in experiments to dissociate amyloid-like fibrils of lyzozyme into its native forms,[47] convert insulin fibrils into soluble monomers, and dissociate a short human thyroid hormone peptide. A simulated laser pulse has also been used in atomistic molecular dynamics simulations to dissociate amyloid fibrils,[48] and to study the breakup of a peptide-based nanotube.[49]

In order to corroborate the results obtained for the 2 × 2 aggregates, we decided to apply the laser melting techniques to the most stable 4 × 2 homopeptide aggregates. For polyN, this is class 1 model 4T3; and for polyQ this is class A model 4O10. Simulations were carried out as outlined in the SI using a laser frequency of 1671 cm^{-1}, which specifically targets the C═O main-chain bonds, thereby destabilizing the β-sheets. The application of this laser pulse results in an almost identical energy absorption for the 4T3 and 4O10 aggregates, as shown in SI Figure S2. However, the structures respond very differently, as shown in Figure 9, which displays two measures of structural integrity: the root-mean-square deviation (RMSD) with respect to the initial, intact structure and the β-sheet content. The behavior of these functions reflects the initial disruption of the hydrogen bonds (to a greater or lesser degree) once the laser pulse is applied, followed by a period of partial healing to the initial structure. For instance, considering the β-sheet content, one notes an initial strong dip in its numerical value as the laser pulse is applied followed by a slower rise to a constant value as the structure attempts to heal itself. For each electric field amplitude, the initial dip and subsequent constant value is systematically lower for 4T3, the most stable polyN structure, than for 4O10, the most stable polyQ structure. Similarly, the RMSDs in Figure 9 are systematically higher for 4T3 than for 4O10. All together, these results indicate that polyQ aggregates are more stable than polyN aggregates.

2.6. The Enthalpic Contributions to the Free Energy Favor PolyQ over PolyN. One can obtain a fairly good estimate of the enthalpic contributions to the free energy of the protofibrils by computing the energy difference between the aggregate and the individual unfolded monomers: $\Delta H = H_{crystal} - 8H_{monomer}$, where $H_{crystal}$ is the enthalpy of the 4 × 2 homopeptide protofibril after equilibration, and $H_{monomer}$ is the average enthalpy of a statistical ensemble of an unfolded monomer, and both terms are computed with the same force field and specifications as described before, but with the Generalized Born approximation for solvation. This gives ΔH_Q = −813 kcal/mol for polyQ 4O10 [approximately −14.5 kcal/ (mol residue)] and ΔH_N = −249 kcal/mol for polyN 4T3 [approximately −4.4 kcal/ (mol residue)].

Clearly, the stability of a β-sheet structure not only depends on the main-chain hydrogen bonds but also on the side-chain packing, associated with both side-chain−side-chain and side-chain−main-chain hydrogen bonds. In order to illustrate the contributions to stability from a structural point of view, we have sketched in Figure 10 the structural differences between the stable models 4T1 (a), 4T3 (b) and 4O10 (c). In the 4T1 model (a), the side chains of two pair of residues Q_4-N_6 of two neighbor chains (A and B or C and D) in the same sheet form hydrogen bonds and create stable polygon structures which support the overall stability of the sheet layer. Additionally, the NE2 atoms of Q_4 residues form hydrogen bonds with the nearest main chains (side-chain−main-chain hydrogen bonds, linking the colored polygons in (a) to the main chains), which contributes to binding

DOI: 10.1021/acschemneuro.5b00337
ACS Chem. Neurosci. 2016, 7, 576−587

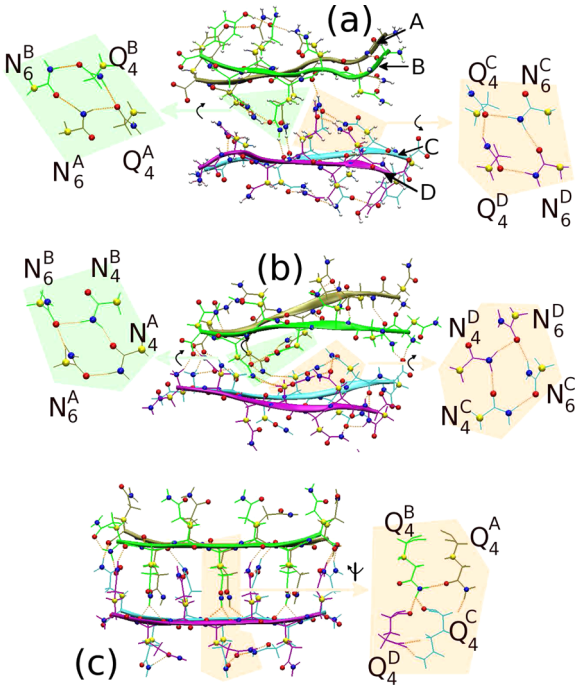

Figure 10. Side-chain packing and hydrogen-bond patterns in 4T1 (a), 4T3 (b), and 4O10 (c) models. Four inner chains labeled A (tan), B (green), C (cyan), and D (purple) are shown. The orange dash lines indicate hydrogen bonds. The N, ND2 (in N-residues), NE2 (in Q-residue) atoms are shown in blue balls. The O, OD1 (in N-residues), OE2 (in Q-residue) atoms are shown in red balls. The CB atoms are shown in yellow balls. The label X_4^A indicates the X-residue (X = Q or N) of the chain A at fourth position (counting the first one from N-terminal for each chain).

the two sheets. In a similar fashion, the two pairs of N_4–N_6 residues in the 4T3 model form polygon structures. However, the interior of the 4T3 model does not exhibit side-chain–main-chain hydrogen bonds. This difference between 4T1 and 4T3 models is most probably due to the length difference between Q and N side chains. The two sheets in the 4T3 model are kept together by hydrogen bonds between the ends of the chains and by the nonstandard hydrogen bonds between ND2 atoms of N_6 (chain A and B) and CB atoms of N_4 (chain C and D). In contrast to the 4T1 and 4T3 models, the polygon side-chain structures allowed by the 2-by-2 packing are not formed in the 1-by-1 4O10 model (Figure 10c). The side-chain packing and hydrogen-bond patterns of the 4O10 model have been discussed in our previous work.[20] In the quarter-stagger conformation of the 4O10 model, an interior Q side chain participates in four hydrogen bonds: two hydrogen bonds with other Q side chains of the nearest chains in the same layer and two other ones with main chain of the nearest layer (Figure 7 in ref 20). The two side-chain–side-chain hydrogen bonds contribute to the stability of the sheet layer, while the two side-chain–main-chain ones not only support binding of the two sheets, but also increase the stability of the nearest sheet. This results in a very stable hydrogen bond network. These structural differences suggest that the shorter side-chain N residues favor 2-by-2 side-chain packing because they can form polygon structures that increase the stability of neighboring sheets, while the longer side-chain Q residues find it advantageous to form side-chain–main-chain hydrogen bonds through 1-by-1 side-chain packing.

2.7. The Entropic Free Energy Difference for the Formation of Steric Zippers Is Higher for PolyQ than for PolyN. The only difference between N and Q is the extra methylene group $-CH_2-$ in the side chain of Q. It is expected therefore that the change in free energy to bring together two strands and form a 2 × 1 β sheet (parallel for N, antiparallel for Q) might be comparable, and indeed a simulation study for a Q_7 pair and a N_7 pair shows very similar free energy profiles in terms of the distance between the strands[37] (with the difference in free energies slightly favoring the formation of the Q_7 pair). In the 2 × 1 β dimers the side chains remain perpendicular to the sheet, free to form occasional hydrogen bonds with the residues or with water. More important differences for the stability of the oligomers may therefore arise from the formation of the steric zipper. Ultimately, as this work shows, polyQ aggregates are more stable than polyN aggregates. Strong enthalpic terms as described before favor the formation of the polyQ aggregates. What about the entropic contribution?

The entropic free energy differences associated with the formation of steric zippers in the two types of peptide can be quickly estimated by considering the degrees of freedom of the side chains (assuming that the backbones have similar degrees of freedom). Asn has 2 side chain torsion angles χ_1 and χ_2, and Gln has 3 side chain torsion angles χ_1, χ_2, and χ_3. The $\{\chi_1\}$ of N and the $\{\chi_1, \chi_2\}$ of Q are defined as rotameric χ's, which exhibit three narrow and symmetric peaks in their density probability distribution. The terminal side-chain torsion angle χ_2 of N and χ_3 of Q is defined as nonrotameric χ, which exhibits a broad and asymmetric probability distribution. The 2002 Rotamer Library[50] defines the degrees of freedom of rotameric χ's as 3 and nonrotameric χ's as 6 for N and Q. The total number of rotamers for the side chains of N and Q therefore becomes 18 and 54 for N and Q in their unfolded states. Since in the aggregate form the side chains are locked into one conformer, the total number of rotamers in the protofibril structure for both peptides is 1. Thus, the entropic loss between a side chain locked in a fibril and a free side chain can be estimated as $\Delta S_Q = S_{Q_{fibril}} - S_{Q_{free}} = -R \ln\left(\frac{54}{1}\right)$ and $\Delta S_N = S_{N_{fibril}} - S_{N_{free}} = -R \ln\left(\frac{18}{1}\right)$. At room temperature (300 K) this gives a difference in entropy favoring the disordered state of $\Delta G_Q = -T\Delta S_Q$ = 2.4 kcal/(mol residue) and $\Delta G_N = -T\Delta S_N$ = 1.73 kcal/(mol residue). (This estimate does not consider the degrees of freedom of the backbones, whose contribution to the free energies is probably similar for polyN and polyQ[37]).

Thus, entropic effects are less favorable to the polyQ steric zippers, as disordered polyQ chains have a more extensive phase space to sample (for n_R residues, the ratio of phase spaces between polyQ and polyN grows as 3^{n_R}) before settling in the preferred conformation. There are probably considerably larger entropic barriers associated with polyQ, which would explain the very long times for the formation of polyQ amyloids observed experimentally.[28,34]

2.8. Other Interspersed Amino Acids Create More Disruption in PolyQ Zippers. Finally, we briefly discuss the effects of other amino acid guests on the stability of the considered structures. Although a systematic study of the effect of every possible amino acid in the N-rich and Q-rich peptides is beyond the scope of this work, there are some observed trends that merit discussion. Aggregates 4T1 and 4T2 indicate that the seven-residue N-rich peptides are tolerant of the terminal G and Y residues, as well as of two inner Q residues. We believe that the 2-by-2 side-chain packing facilitates the accommodation of these

DOI: 10.1021/acschemneuro.5b00337
ACS Chem. Neurosci. 2016, 7, 576–587

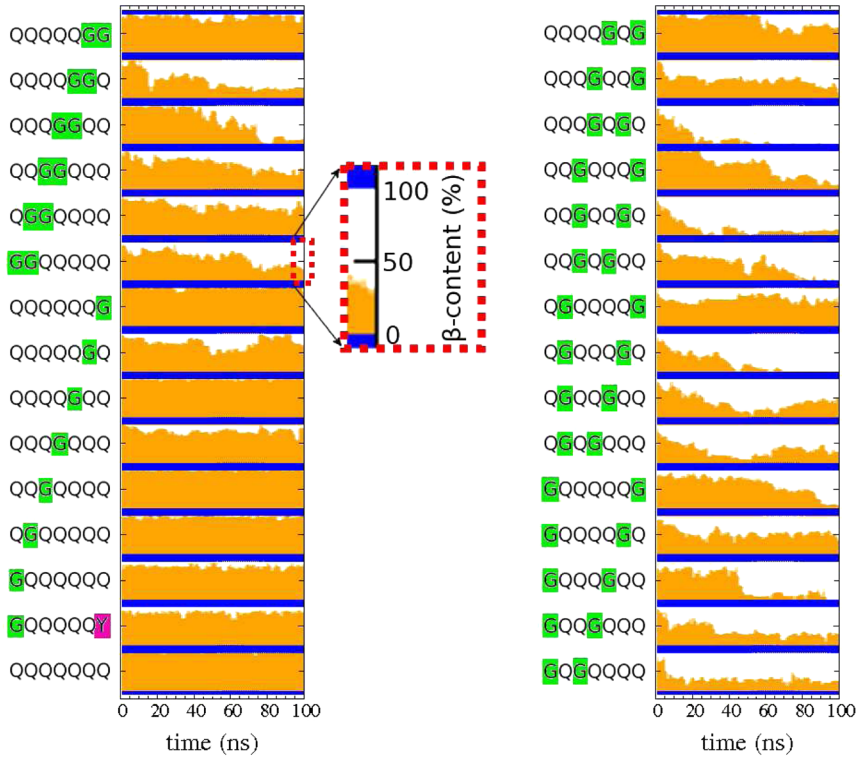

Figure 11. Dynamic evolution of the β-sheet content of all possible mutations of the 2 × 2 2010 class A structure (QQQQQQQ) based on mutating one or two Qs into Gs. The time evolution of the β-content is plotted in orange. The mutated residues Gly (G) and Tyr (Y) on the different sequences are marked in green and purple, respectively. The blue lines separate the different models.

other amino acids. However, Q-rich peptides prefer 1-by-1 side-chain packing. Thus, 4 × 2 parallel arrangements such as 4O2 and 4O4 for Q_7 are stable, but the 4 × 2 parallel model 4T4 for GQ_5Y is not. On the other hand, the presence of the terminal G and Y in GQ_5Y only slightly diminishes the β-sheet content with respect to Q_7 (Figure 11) when the peptides are in class A, which indicates that the structures may be more tolerant of terminal substitutions.

Since polyQ prefers a class A steric zipper, we investigated the effects of G substitutions in the 2010 polyQ aggregates, in order to probe the effect of a guest amino acid on the stability of these structures. Figure 11 shows that single G residues only moderately decrease the β-sheet content with respect to Q_7, in a position-dependent manner. On the other hand, two G residues cause considerable disruption that strongly depends on the position of these residues.

PolyQ fibrils are characterized by the carefully balanced stacking of the side chains,[16,20] that maximizes the dipolar, hydrogen-bond, and van der Waals contacts. Thus, the presence of other amino acids will generally disrupt these contacts. The sensitivity of polyQ amyloid formation to the presence of other amino acids is displayed even in less intuitive cases. For instance, flanking sequences play a structural role in pure polyQ sequences, both in synthetic and natural peptides. A polyproline (polyP) region immediately adjacent to the C-terminal of a polyQ region has been shown to affect the conformation of the polyQ region; the resulting conformations depend on the lengths of both the polyQ and polyP sequences.[51] Even for monomeric, disordered Q_{40} a C-terminal hexaproline suppresses both the population of "rare motifs" and the long-range correlation of the dihedral angles present in Q_{40} without the hexaproline.[7]

3. CONCLUSIONS

In summary, we have carried out the first comprehensive theoretical study based on MD simulations of all the possible steric interfaces of important N/Q-rich peptides forming amyloids, especially sequences as found in the yeast Sup35 prion domain. We have compared the structural characteristics and thermodynamic stability of these protofibril aggregates in prion-like proteins. Specifically, we explored all possible steric zipper interfaces for N-rich and Q-rich oligomers in order to determine which crystallographic class provides the most stability to the N-rich or Q-rich fibril precursor. Our observations can be summarized as follows. First, different crystal classes maximize stability in N-rich or Q-rich aggregates: N-rich oligomers are most stable in parallel-stranded β-sheets with 2-by-2 side-chain interdigitation (model 4T3), while polyQ oligomers are most stable in antiparallel-stranded β-sheets with 1-by-1 steric zippers (model 4O10). Our results show that the polyQ 4O10 model is more stable than the polyN 4T3 model. Enthalpic contributions to the free energy favor the formation of polyQ protofibrils, while entropic contributions favor the formation of polyN protofibrils. The presence of β-hairpin turns in polyN leading to β-sheets not necessarily explains the observed trend of polyN faster aggregation, since N-rich sequences tend to favor parallel β-sheets, as opposed to antiparallel ones, and β-hairpin turns are more stable in polyQ than in polyN. The considerably larger phase space that disordered polyQ must sample on its way to aggregation probably is at the root of the associated slower kinetics observed experimentally. When other amino acids are present, such as in the Sup35 PrD, their shorter side chains favor steric-zipper formation for N but not Q, as they preclude the in-register association of the long Q side chains.

DOI: 10.1021/acschemneuro.5b00337
ACS Chem. Neurosci. 2016, 7, 576−587

4. METHODS

4.1. Molecular Dynamics Simulations. The simulations were carried out with the AMBER 12 simulation package[52] with the ff12SB force field. The TIP3P water model was used for the explicit solvent simulations with periodic boundary conditions in orthorhombic boxes (more than 7000 waters for the hairpins, 6000 for the 4 × 2 systems and 4500 for the 2 × 2 systems). The construction of the initial models and the equilibration procedures are described in the SI. Electrostatics were handled by the PME method,[53] with a direct space cutoff of 9 Å, and with an average mesh size of approximately 1 Å for the lattice calculations. We used Langevin dynamics with a coupling parameter $\gamma = 1.0\ ps^{-1}$. The NPT simulations were carried out mainly at 300 K and 1 atm via the Berendsen barostat with an isothermal compressibility of $\beta = 44.6 \times 10^{-6}\ bar^{-1}$ and pressure relaxation time $\tau_p = 1.0$ ps. The length of the simulation was 100 ns for the hairpins and 2 × 2 systems and 400 ns for the 4 × 2 systems. Finally, for each of the systems we carried out 10 independent runs. We tracked the RMSDs with respect to the initial structures (after equilibration) and the β-sheet content of the aggregates as a function of time. We also tracked the interstrand and intersheet distances as a function of time. The definition of these two distances as well as the corresponding results are presented in the SI.

4.2. Laser Melting Simulations. While most of our conclusions are based on MD simulations in explicit waters, we have carried out a limited number of nonequilibrium MD simulations in which the structures were subject to a laser pulse with an electric field:

$$E(t) = E_0 \exp\left[-\frac{(t - t_0)^2}{2\sigma^2}\right]\cos[2\pi c\omega(t - t_0)]$$

where E_0 indicates the modulus of the electric field amplitude, σ the pulse width, t the time after the pulse maximum t_0, c the speed of light, and ω the frequency. Such a classical laser pulse is characteristic of a free-electron based laser[46,47] with specific oscillation characteristics of a picosecond pulse structure, tunable wavelengths within the infrared regime, and a high photon density. Using this laser pulse, it has been possible to target specific bonds within a given structure and thereby study the unfolding of the structure. Specifically, this method was used to investigate the dissociation of amyloid fibrils into soluble monomers,[47,48] and the breakup of a peptide-based nanotube.[49] Here, we use such nonequilibrium MD simulations simply as an alternative way of exploring the relative stability of a given set of structures. Thus, by tuning the laser frequency to target key bonds that hold the structure together, the structure can be disrupted. According to the field intensity, the broken bonds may or may not reconnect. The application of such a laser pulse causes localized damage to the stable structure, given that all other conditions and parameters are equal. For our purposes, we use these laser pulse simulations simply as a tool to examine the relative stability of the polyN and polyQ most stable models (4T3 and 4O10), and do not focus on the microscopics of the laser melting. We emphasize here that these laser melting simulations are not needed per se, but are given because they lend additional support to stability results as obtained with the other MD simulations. Details of these laser pulse simulations and their analysis are relegated to the SI.

■ ASSOCIATED CONTENT

Supporting Information

The Supporting Information is available free of charge on the ACS Publications website at DOI: 10.1021/acschemneuro.5b00337.

Further details on simulations and analysis, frequency dependence of structures, infrared laser energy differences, intersheet and interstand distances for models, RMSD for models, and β-content for different models (PDF)

■ AUTHOR INFORMATION

Corresponding Author

*E-mail: sagui@ncsu.edu. Phone: 919-515-3111.

Author Contributions

Y.Z. and V.H.M. ran simulations; Y.Z. and V.H.M. analyzed data; all authors helped formulate problem and wrote paper.

Funding

This work has been supported by the National Science Foundation (NSF) via SI2-SSE-1148144 and 1534941.

Notes

The authors declare no competing financial interest.

■ ACKNOWLEDGMENTS

We also thank the NC State HPC and especially the XSEDE TG-MCB150114 for computational support.

■ REFERENCES

(1) Golding, G. B. (1999) Simple sequence is abundant in eukaryotic proteins. *Protein Sci. 8*, 1358−61.

(2) Faux, N. G., Bottomley, S. P., Lesk, A. M., Irving, J. A., Morrison, J. R., de la Banda, M. G., and Whisstock, J. C. (2005) Functional insights from the distribution and role of homopeptide repeat-containing proteins. *Genome Res. 15*, 537−551.

(3) Le Gall, T., Romero, P. R., Cortese, M. S., Uversky, V. N., and Dunker, A. K. (2007) Intrinsic disorder in the Protein Data Bank. *J. Biomol. Struct. Dyn. 24*, 325−341.

(4) Bonen, L., Haerty, W., and Golding, G. B. (2010) Low-complexity sequences and single amino acid repeats: not just "junk" peptide sequences. *Genome 53*, 753−762.

(5) Mukhopadhyay, S., Krishnan, R., Lemke, E. A., Lindquist, S., and Deniz, A. A. (2007) A natively unfolded yeast prion monomer adopts an ensemble of collapsed and rapidly fluctuating structures. *Proc. Natl. Acad. Sci. U. S. A. 104*, 2649−2654.

(6) Toombs, J. A., McCarty, B. R., and Ross, E. D. (2010) Compositional determinants of prion formation in yeast. *Mol. Cell. Biol. 30*, 319−332.

(7) Moradi, M., Babin, V., Roland, C., and Sagui, C. (2012) Are long-range structural correlations behind the aggregation phenomena of polyglutamine diseases? *PLoS Comput. Biol. 8*, e1002501.

(8) Perutz, M. F., Pope, B. J., Owen, D., Wanker, E. E., and Scherzinger, E. (2002) Aggregation of proteins with expanded glutamine and alanine repeats of the glutamine-rich and asparagine-rich domains of Sup35 and of the amyloid beta-peptide of amyloid plaques. *Proc. Natl. Acad. Sci. U. S. A. 99*, 5596−5600.

(9) Uversky, V. N. (2008) Amyloidogenesis of natively unfolded proteins. *Curr. Alzheimer Res. 5*, 260−287.

(10) Davies, S. W., Turmaine, M., Cozens, B. A., DiFiglia, M., Sharp, A. H., Ross, C. A., Scherzinger, E., Wanker, E. E., Mangiarini, L., and Bates, G. P. (1997) Formation of neuronal intranuclear inclusions underlies the neurological dysfunction in mice transgenic for the HD mutation. *Cell 90*, 537−548.

(11) Fiumara, F., Fioriti, L., Kandel, E. R., and Hendrickson, W. A. (2010) Essential role of coiled coils for aggregation and activity of Q/N-rich prions and PolyQ proteins. *Cell 143*, 1121−1135.

(12) Perutz, M. F., Finch, J. T., Berriman, J., and Lesk, A. (2002) Amyloid fibers are water-filled nanotubes. *Proc. Natl. Acad. Sci. U. S. A. 99*, 5591−5595.

(13) Daggett, V. (2006) α-Sheet: The toxic conformer in amyloid diseases? *Acc. Chem. Res. 39*, 594−602.

(14) Babin, V., Roland, C., and Sagui, C. (2011) The α-sheet: A missing-in-action secondary structure? *Proteins: Struct., Funct., Genet. 79*, 937−946.

(15) Sharma, D., Shinchuk, L. M., Inouye, H., Wetzel, R., and Kirschner, D. A. (2005) Polyglutamine homopolymers having 8−45 residues form slablike beta-crystallite assemblies. *Proteins: Struct., Funct., Genet. 61*, 398−411.

(16) Sikorski, P., and Atkins, E. (2005) New model for crystalline polyglutamine assemblies and their connection with amyloid fibrils. *Biomacromolecules 6*, 425−432.

DOI: 10.1021/acschemneuro.5b00337
ACS Chem. Neurosci. 2016, 7, 576−587

(17) Schneider, R., Schumacher, M. C., Mueller, H., Nand, D., Klaukien, V., Heise, H., Riedel, D., Wolf, G., Behrmann, E., Raunser, S., Seidel, R., Engelhard, M., and Baldus, M. (2011) Structural characterization of polyglutamine fibrils by solid-state NMR spectroscopy. *J. Mol. Biol. 412*, 121−136.
(18) Buchanan, L. E., Carr, J. K., Fluitt, A. M., Hoganson, A. J., Moran, S. D., de Pablo, J. J., Skinner, J. L., and Zanni, M. T. (2014) Structural motif of polyglutamine amyloid fibrils discerned with mixed-isotope infrared spectroscopy. *Proc. Natl. Acad. Sci. U. S. A. 111*, 5796−801.
(19) Kar, K., Hoop, C. L., Drombosky, K. W., Baker, M. A., Kodali, R., Arduini, I., van der Wel, P. C., Horne, W. S., and Wetzel, R. (2013) β-hairpin-mediated nucleation of polyglutamine amyloid formation. *J. Mol. Biol. 425*, 1183−1197.
(20) Man, V. H., Roland, C., and Sagui, C. (2015) Structural determinants of polyglutamine protofibrils and crystallites. *ACS Chem. Neurosci. 6*, 632−645.
(21) Prusiner, S. B. (1998) Prions. *Proc. Natl. Acad. Sci. U. S. A. 95*, 13363−13383.
(22) True, H. L., and Lindquist, S. L. (2000) A yeast prion provides a mechanism for genetic variation and phenotypic diversity. *Nature 407*, 477−83.
(23) Coustou, V., Deleu, C., Saupe, S., and Begueret, J. (1997) The protein product of the het-s heterokaryon incompatibility gene of the fungus Podospora anserina behaves as a prion analog. *Proc. Natl. Acad. Sci. U. S. A. 94*, 9773−9778.
(24) Sawyer, E. B., Claessen, D., Haas, M., Hurgobin, B., and Gras, S. L. (2011) The assembly of individual chaplin peptides from Streptomyces coelicolor into functional amyloid fibrils. *PLoS One 6*, e18839.
(25) Barnhart, M. M., and Chapman, M. R. (2006) Curli biogenesis and function. *Annu. Rev. Microbiol. 60*, 131−47.
(26) Peters, T. W., and Huang, M. (2007) Protein aggregation and polyasparagine-mediated cellular toxicity in Saccharomyces cerevisiae. *Prion 1*, 144−153.
(27) Michelitsch, M. D., and Weissman, J. S. (2000) A census of glutamine/asparagine-rich regions: Implications for their conserved function and the prediction of novel prions. *Proc. Natl. Acad. Sci. U. S. A. 97*, 11910−11915.
(28) Halfmann, R., Alberti, S., Krishnan, R., Lyle, N., O'Donnell, C. W., King, O. D., Berger, B., Pappu, R. V., and Lindquist, S. (2011) Opposing effects of glutamine and asparagine govern prion formation by intrinsically disordered proteins. *Mol. Cell 43*, 72−84.
(29) Miller, J., Arrasate, M., Shaby, B. A., Mitra, S., Masliah, E., and Finkbeiner, S. (2010) Quantitative relationships between Huntingtin levels, polyglutamine length, inclusion body formation, and neuronal death provide novel insight into Huntingtonas disease molecular pathogenesis. *J. Neurosci. 30*, 10541−10550.
(30) Arrasate, M., Mitra, S., Schweitzer, E. S., Segal, M. R., and Finkbeiner, S. (2004) Inclusion body formation reduces levels of mutant huntingtin and the risk of neuronal death. *Nature 431*, 805−810.
(31) Ross, C. A., and Poirier, M. A. (2005) What is the role of protein aggregation in neurodegeneration? *Nat. Rev. Mol. Cell Biol. 6*, 891−898.
(32) Si, K., Lindquist, S. L., and Kandel, E. R. (2003) A neuronal isoform of the aplysia CPEB has prion-like properties. *Cell 115*, 879−891.
(33) Ross, E. D., Minton, A., and Wickner, R. B. (2005) Prion domains: sequences, structures and interactions. *Nat. Cell Biol. 7*, 1039−1044.
(34) Lu, X., and Murphy, R. M. (2015) Asparagine repeat peptides: aggregation kinetics and comparison with glutamine repeats. *Biochemistry 54*, 4784−94.
(35) Sawaya, M. R., Sambashivan, S., Nelson, R., Ivanova, M. I., Sievers, S. A., Apostol, M. I., Thompson, M. J., Balbirnie, M., Wiltzius, J. J. W., McFarlane, H. T., Madsen, A. ø., Riekel, C., and Eisenberg, D. (2007) Atomic structure of amyloid cross-β spines reveal varied steric zippers. *Nature 447*, 453−457.
(36) Zhang, Y., and Sagui, C. (2015) Secondary structure assignment for conformationally irregular peptides: Comparison between DSSP, STRIDE and KAKSI. *J. Mol. Graphics Modell. 55*, 72−84.
(37) Nakano, M., Ebina, K., and Tanaka, S. (2013) Study of the aggregation mechanism of polyglutamine peptides using replica exchange molecular dynamics simulations. *J. Mol. Model. 19*, 1627−1639.
(38) Nelson, R., Sawaya, M. R., Balbirnie, M., Madsen, A. O., Riekel, C., Grothe, R., and Eisenberg, D. (2005) Structure of the cross-β spine of amyloid-like fibrils. *Nature 435*, 773−778.
(39) Gsponer, J., Haberthür, U., and Caflisch, A. (2003) The role of side-chain interactions in the early steps of aggregation: Molecular dynamics simulations of an amyloid-forming peptide from the yeast prion Sup35. *Proc. Natl. Acad. Sci. U. S. A. 100*, 5154−5159.
(40) Vitagliano, L., Esposito, L., Pedone, C., and De Simone, A. (2008) Stability of single sheet GNNQQNY aggregates analyzed by replica exchange molecular dynamics: antiparallel versus parallel association. *Biochem. Biophys. Res. Commun. 377*, 1036−1041.
(41) Balbirnie, M., Grothe, R., and Eisenberg, D. S. (2001) An amyloid-forming peptide from the yeast prion Sup35 reveals a dehydrated β-sheet structure for amyloid. *Proc. Natl. Acad. Sci. U. S. A. 98*, 2375−2380.
(42) Shewmaker, F., Wickner, R. B., and Tycko, R. (2006) Amyloid of the prion domain of Sup35p has an in-register parallel β-sheet structure. *Proc. Natl. Acad. Sci. U. S. A. 103*, 19754−19759.
(43) De Simone, A., Esposito, L., Pedone, C., and Vitagliano, L. (2008) Insights into stability and toxicity of amyloid-like oligomers by replica exchange molecular dynamics analyses. *Biophys. J. 95*, 1965−1973.
(44) Richardson, J. S., and Richardson, D. C. (2002) Natural β-sheet proteins use negative design to avoid edge-to-edge aggregation. *Proc. Natl. Acad. Sci. U. S. A. 99*, 2754−2759.
(45) Laidman, J., Forse, G. J., and Yeates, T. O. (2006) Conformational change and assembly through edge beta strands in transthyretin and other amyloid proteins. *Acc. Chem. Res. 39*, 576−583.
(46) Yagi, H., Ozawa, D., Sakurai, K., Kawakami, T., Kuyama, H., Nishimura, O., Shimanouchi, T., Kuboi, R., Naiki, H., and Goto, Y. (2010) Laser-induced propagation and destruction of amyloid beta fibrils. *J. Biol. Chem. 285*, 19660.
(47) Kawasaki, T., Fujioka, J., Imai, T., and Tsukiyama, K. (2012) Effect of mid-infrared free-electron laser irradiation on refolding of amyloid-like fibrils of Lysozyme into native form. *Protein J. 31*, 710.
(48) Man, V. H., Derreumaux, P., Li, M. S., Roland, C., Sagui, C., and Nguyen, P. (2015) Picosecond dissociation of amyloid fibrils with infrared laser: A nonequilibrium simulation study. *J. Chem. Phys. 143*, 155101.
(49) Man, V., Truong, P., Derreumaux, P., Li, M., Roland, C., Sagui, C., and Nguyen, P. (2015) Picosecond Melting of Peptide Nanotube with Infrared Laser: A Nonequilibrium Study. *Phys. Chem. Chem. Phys. 17*, 27275−80.
(50) Dunbrack, R. L., Jr. (2002) Rotamer Libraries in the 21st Century. *Curr. Opin. Struct. Biol. 12*, 431−440.
(51) Darnell, G. D., Derryberry, J., Kurutz, J. W., and Meredith, S. C. (2009) Mechanism of Cis-inhibition of polyQ fibrillation by polyP: PPII oligomers and the hydrophobic effect. *Biophys. J. 97*, 2295−2305.
(52) Case, D. A. et al. *AMBER 12*; University of California: San Francisco, 2012.
(53) Essmann, U., Perera, L., Berkowitz, M. L., Darden, T., Lee, H., and Pedersen, L. G. (1995) A smooth particle mesh Ewald method. *J. Chem. Phys. 103*, 8577−8593.

DOI: 10.1021/acschemneuro.5b00337
ACS Chem. Neurosci. 2016, 7, 576−587